Research Square

Preprints are preliminary reports that have not undergone peer review.
They should not be considered conclusive, used to inform clinical practice,
or referenced by the media as validated information.

# Geomechanical Stability Assessment of Underground Chalk Heritage Galleries Based on TLS-Derived 3D Geometry and Numerical Modelling

**Mateusz Blajer**

blajer@agh.edu.pl

AGH University of Krakow

**Wioletta Podwyszyńska-Sałosz**

Budimex (Poland)

**Krzysztof Tajduś**

AGH University of Krakow

**Article**

**Keywords:** terrestrial laser scanning (TLS), three-dimensional numerical modelling, underground chalk workings

**Posted Date:** October 29th, 2026

**DOI:** https://doi.org/10.21203/rs.3.rs-11320072/v1

**License:** This work is licensed under a Creative Commons Attribution 4.0 International License.
Read Full License

**Additional Declarations:** No competing interests reported.

# Abstract

The aim of this study was to assess the stability of selected chambers within the historic chalk underground workings using advanced three-dimensional computational methods. A numerical model was developed based on terrestrial laser scanning data. Strength and deformation tests were conducted on chalk samples to determine the parameters of the constitutive model. The stability analysis of selected chambers beneath the market square in Chełm identified potential zones characterised by low stability indices. Furthermore, the analysis revealed the most highly stressed sections of the underground workings.


# Introduction

Historic underground excavations in weak and porous rocks constitute a distinct class of geotechnical structures in which instability risk results from the combined effects of complex geometry, heterogeneous rock-mass degradation, and long-term environmental influences. The Chełm Chalk Tunnels are a unique monument of historic Polish chalk mining. Their intensive development took place during the sixteenth and seventeenth centuries and ceased only in the nineteenth century, when the extensive network of underground passages began to pose a significant threat to local residents. The excavations were created in writing chalk, which exhibits relatively favourable strength and deformation properties at low moisture contents. However, owing to its high porosity and hygroscopic nature, the material undergoes marked degradation as its moisture content increases. Water ingress disrupts its cohesion and microstructure, promoting layer detachment and displacement as well as roof collapse, even under relatively low loads. Consequently, failure mechanisms may develop that lead to the load-bearing capacity of pillars and roofs being exceeded, the initiation of stress-arching effects, and the propagation of discontinuous ground deformations. In extreme cases, these processes may manifest as sinkholes and damage to structures at the ground surface.

The significance of weathering and moisture-related processes in chalk has been clearly demonstrated in international studies. Lafrance et al. [1] showed that progressive weathering and moisture ingress can nearly double the reduction in strength parameters, thereby decreasing the stability indices of entire chambers within abandoned underground workings. A similar analytical approach was applied to the shallow Malogne chalk mine in Belgium, where geological characterisation, mechanical testing under dry and saturated conditions, and numerical modelling were combined to identify zones with an elevated risk of collapse [2, 3]. The literature also emphasises that empirical methods may significantly overestimate safety in mining and cultural heritage structures characterised by irregular geometries. For example, an analysis of the abandoned Bodovalle mine [4] revealed differences exceeding a factor of two between empirical and numerical modelling results, with the empirical methods producing less conservative estimates. This finding has direct implications for risk management and the selection of preventive measures.

In recent years, the integration of high-resolution geometric data acquired using terrestrial laser scanning (TLS) or structure-from-motion photogrammetry (SfM) with three-dimensional numerical models calibrated against laboratory test results has become well established. Advances have been made in both the representation of excavation geometry and discontinuities and the quality of input data used to generate computational meshes. These developments include methods for correcting laser-scanning intensity data in underground environments [5] and integrating survey results with diagnostic assessments of heritage structures [6]. The effectiveness of the scan-to-FEM approach was demonstrated, among others, for the Sabereebi complex in Georgia [7]. In that study, high-resolution three-dimensional finite element models incorporating an elastoplastic Mohr–Coulomb failure criterion and a shear-strength reduction procedure were used. Bedding and discontinuities were included to identify stress-concentration zones and potential instability scenarios. Similarly, a study of the Yuanjue Cave [8] highlighted the importance of accurately representing rock structure and weathering-induced voids when assessing roof-bearing capacity. It should be noted, however, that local numerical indications of instability do not necessarily imply global stability loss and must be interpreted in the context of the relevant failure mechanism and uncertainties in the input data [9].

A major challenge associated with chalk is the selection of a constitutive model capable of accounting for strain-rate dependence and rheological processes, which may control the long-term evolution of stress and deformation fields. Viscoplastic models developed for chalk and other porous rocks [10, 11] indicate that reliable predictions require the simultaneous representation of shear-induced failure, strain-rate-dependent pore-collapse mechanisms, and their coupling with moisture conditions. In engineering practice and analyses of historic underground structures, a staged approach is commonly adopted. This involves calibrating material parameters using strength and deformation tests on laboratory specimens, characterising the rock mass using systems such as RMR or GSI, and conducting three-dimensional analyses based on TLS-derived geometry, supplemented by sensitivity analyses addressing moisture conditions and material degradation.

The present study follows this methodological framework: laser scanning → 3D reconstruction → identification of geological units and discontinuities → laboratory testing → calibration of the constitutive model → 3D analysis and mapping of critical zones. The primary objective is to assess the stability of selected chambers within the chalk underground workings beneath the market square in Chełm using advanced three-dimensional computational methods. The study also aims to identify potential zones characterised by reduced stability indices and the most highly stressed sections of the excavations, thereby providing a basis for designing monitoring programmes and preventive measures. The principal contribution of this study lies in the consistent integration of TLS data, the geomechanical characterisation of chalk—including the effects of moisture—and three-dimensional numerical analysis focused on the practical assessment of geohazards within historic underground workings.

# Results

### Numerical Stability Assessment of the Analysed Section of the Chalk Underground Workings

Stability was assessed using a three-dimensional approach that simultaneously considered the response of the rock mass to surface loads from buildings and vehicular traffic and the behaviour of the selected unsupported chambers and underground workings. The results are presented as displacement fields, factor-of-safety (FS) maps, and strength–stress ratio (SSR) maps for two in situ stress-field scenarios defined by mean lateral earth-pressure coefficients of $\bar{\lambda}$=0.8 and $\bar{\lambda}$=1.2.

**Surface Stability Maps**

The surface FS maps (Fig. 1) indicate that the study area currently exhibits an adequate safety margin under both $\bar{\lambda}$. scenarios.

The literature indicates that FS = 2.0 may be adopted as a reference value under conditions comparable to those analysed in this study. Accordingly, this value was adopted as the minimum acceptable safety level for both the surface structures and the analysed chambers.

The calculated surface FS distributions do not indicate a critical condition. Their interpretation must, however, account for the long-term evolution of the hydrogeological conditions. Progressive weathering and increasing moisture content within chalk rock masses may cause a gradual reduction in strength and deformation parameters, consequently decreasing the FS. Moreover, more detailed ground investigations, such as exploratory drilling, may reveal weakened zones within the geological profile—particularly at shallow depths—that are not represented in the current generalised model and could significantly affect the stability assessment. The SSR maps indicate that local fractured zones, approximately 50–60 cm thick, develop around the excavations. This finding is consistent with the chalk detachments observed in the roofs and sidewalls during the field survey (Fig. 2).

**Total Displacements**

The total displacement magnitudes within the chambers (Fig. 3 and Supplementary Fig. S1) range from 0 to 0.008 m. The $\bar{\lambda}$ = 0.8 scenario produces lower displacement values: approximately 0.004 m along the sidewalls and 0.007–0.008 m at the excavation floor, particularly in the vicinity of the “Bieluch” Chamber. For $\bar{\lambda}$ = 1.2, more pronounced sidewall displacements are observed, locally extending into the floor zones.

A characteristic feature of both scenarios is the occurrence of localised displacement maxima at the chamber floors. These may indicate local strain concentrations associated with geometric irregularities or with constrictions and intersections.

**Strength–Stress Ratio in the Selected Chambers**

The strength–stress ratio SSR was analysed in sections P1, P2, and P4 (Fig. 4), with particular attention paid to zones in which the SSR approaches 1.0, where a value of 1.0 denotes failure.

The optimal excavation profile should approximate an ellipse whose major and minor diameters correspond to the major and minor stresses acting within the rock mass. Given the observed geometry of the analysed chambers (Supplementary Fig. S2), in which the vertical diameter is generally greater than the horizontal diameter, a corresponding relationship between the horizontal and vertical stresses, with $\bar{\lambda}$< 1.0, would be expected.

For section P1 under the $\bar{\lambda}$ = 0.8 scenario (Fig. 2a), the high stress-utilisation zones develop primarily along the sidewalls, reaching a local thickness of 60–70 cm, whereas only isolated zones occur in the roof. In section P2, which intersects four chambers (Fig. 5a), the sidewall zones characterised by SSR ≈ 1.0 are 18–48 cm thick for $\bar{\lambda}$ = 0.8. A thin zone approximately 12 cm thick also occurs in the roof of the lowermost chamber, whereas no zones with SSR ≈ 1.0 develop at the chamber floors.

Increasing $\bar{\lambda}$ to 1.2 results in greater stress utilisation within the roofs and floors, where the affected zones are 8–25 cm thick (Figs. 2b and 5b), while simultaneously reducing the extent of the affected sidewall zones to 12–43 cm. This indicates stress redistribution: the greater contribution of horizontal stresses reduces the loading of the sidewalls at the expense of increased stress utilisation in the roofs and floors. This response most likely results from the geometry of most of the analysed excavations being better suited to conditions in which $\bar{\lambda}$ < 1.0.

In section P4, the lowermost chamber, located beneath approximately 15 m of overburden, is of particular importance.

Even under the $\bar{\lambda}$ = 0.8 scenario, zones with SSR ≈ 1.0 occur in the roof and floor, extending to a depth of 20 cm, and along the sidewalls, where they extend to 30 cm (Fig. 6a). For $\bar{\lambda}$ = 1.2, the extent of these zones increases to 45–55 cm, indicating that the deepest parts of the analysed workings are more sensitive to this stress-field scenario (Fig. 6b).

**Factor-of-Safety (FS) Maps for the Analysed Chambers**

The factor-of-safety maps for the chambers (Fig. 7) indicate minimum FS values of 2.13 for $\bar{\lambda}$ = 0.8 and 2.16 for $\bar{\lambda}$ = 1.2. Both values exceed the adopted minimum acceptable threshold of FSmin = 2.0.

These results indicate that, under the conditions adopted in the model, there is no evidence of global instability in the analysed chambers. Nevertheless, the SSR distributions indicate the potential presence of localised weakened zones, particularly along the sidewalls and, under the $\bar{\lambda}$ = 1.2 scenario, also within the roofs and floors of selected chambers. This finding is consistent with field observations of small chalk blocks detaching from the excavation surfaces.

# Discussion

The scan-to-model methodology adopted in this study, combining TLS-based geometry reconstruction, geomechanical parameterisation based on laboratory tests, and three-dimensional numerical analysis, enabled the stability of historic underground workings with highly irregular geometries to be assessed.

The results indicate that the analysed chambers remain globally stable, with FS > 2.0 (under both $\bar{\lambda}$ scenarios), while the SSR maps reveal localised zones of elevated stress utilisation. Such behaviour is typical of shallow underground voids excavated in weak porous rocks, where deterioration is more likely to result from local mechanisms, such as block detachment and delamination, than from an immediate large-scale collapse.

The chambers were probably excavated towards an optimal geometry that maximised stability, with their profiles progressively adjusted based on observations of the excavation-boundary response. In this context, the FS alone is insufficient for a comprehensive interpretation of stability. Mapping and analysing the extent of zones in which SSR ≈ 1.0, and comparing them with the locations of rock detachments observed during the field survey, are therefore essential.

The sensitivity analysis of the adopted in situ stress field ( $\bar{\lambda}$ = 0.8 vs $\bar{\lambda}$ = 1.2) revealed substantial redistribution of stress utilisation. At the higher $\bar{\lambda}$ value, the sidewalls are unloaded, whereas stress utilisation increases in the roofs and floors of selected chambers. Mechanically, this represents a change in the dominant damage scenario, which is relevant to support design because it shifts the reinforcement priority between the sidewalls and the roofs.

At the same time, the limited ground-surface displacements suggest that there is currently no threat to the serviceability of the overlying buildings under the analysed conditions. This result should nevertheless be interpreted with caution because the model does not account for historical collapses or secondary infill materials, which may have locally altered the rock-mass stiffness and patterns of strain concentration.

The greatest source of uncertainty concerns the effects of moisture and weathering. Laboratory tests confirmed that the material parameters are strongly dependent on moisture conditions. However, time-dependent processes, including moisture-induced degradation and creep, were not explicitly incorporated into the model. The calculated FS values should therefore be interpreted as an assessment of the current condition under the adopted parameter set.

The proposed scan-to-model methodology can be applied to assess the stability of historic underground workings with complex geometries and to support the planning of monitoring and reinforcement measures.

# Methods

### Geological and Engineering Conditions in the Study Area

The chalk deposits in the vicinity of Chełm were formed during the Cretaceous, the youngest period of the Mesozoic Era, following the Jurassic and preceding the Cenozoic Era (Tertiary–Palaeocene) [12]. A review of historical geological data, supplemented by a recent analysis of lithological borehole logs, confirmed that Quaternary deposits in the area of the underground museum extend to depths ranging

from 1.0 to 5.0 m. These deposits are underlain by writing chalk extending to the bottom of the exploratory boreholes, the deepest of which reached 122 m. The chalk deposits form nearly horizontal strata. The investigations also revealed a predominant NE–SE orientation of fractures intersecting the individual chalk beds [12]. A schematic geological profile developed from the investigation results is presented in Supplementary Fig. S3.

Three zones exhibiting different degrees and forms of weathering were identified within the chalk deposits. The uppermost zone, extending to a depth of approximately 2 m, consists of fine rock debris with fragments several centimetres in size. The intermediate zone, located at depths of approximately 2–6 m, comprises chalk blocks measuring less than 1 m. In the deepest zone, weathering processes are observed only along fracture surfaces.

**Laboratory Testing and Rock-Mass Parameterisation for the Numerical Model**

To calibrate the physical and mechanical parameters, blocks of writing chalk measuring approximately 60 × 30 × 30 cm were collected from the vicinity of the Tourist Route and the analysed section of the underground workings. The material was preserved at its natural moisture content and stored under conditions that minimised drying until the cylindrical specimens were prepared. The natural moisture content $w_n$ and unit weight γ, were determined in accordance with the ISRM recommendations [13]. The remaining tests were conducted using procedures adapted to the brittle, porous, and highly water-sensitive structure of the chalk; any deviations from the standard procedures are described later in this paper. For the subsequent deformability analyses, the secant modulus $E_{50}$ was adopted as the parameter considered most representative of weak porous rocks. The laboratory test results are summarised in Table 1.

Table 1
Physical and mechanical parameters determined from laboratory tests

| Parameter | Range | Mean | Median |
|---|---|---|---|
| Unit weight γ [kN/m$^3$] | 18.91–19.44 | 19.08 | 19.06 |
| Tensile strength $R_{r,wn}$ [MPa] | 0.22–0.37 | 0.29 | 0.29 |
| Uniaxial compressive strength $R_{c,wn}$ [MPa] | 1.47–3.18 | 2.10 | 1.94 |
| Uniaxial compressive strength $R_{c,s}$ [MPa] | 4.88–14.16 | 8.23 | 7.71 |
| Secant strain modulus $E_{50,wn}$ [MPa] | 167.96–747.74 | 370.92 | 363.85 |
| Secant strain modulus $E_{50,s}$ [MPa] | 532.36–1725.11 | 1035.82 | 1065.58 |
| Subscripts: wn—natural moisture content; s—after drying | | | |

**Physical and Mechanical Properties**

The unit weight was determined for 30 specimens at their natural moisture content and exhibited limited variability, ranging from 18.91 to 19.44 kN/m³. Greater variability was recorded for the strength parameters, particularly the uniaxial compressive strength of specimens dried to a constant mass. Writing chalk is described as a rock exhibiting exceptionally high homogeneity at the laboratory scale. Nevertheless, its physical and mechanical properties may vary considerably as a result of sedimentary and diagenetic processes [14]. Chalk may therefore exhibit various forms of heterogeneity that are significant from both geological and geotechnical perspectives, as extensively discussed by Faÿ et al. and Jeans et al. [15, 16].

The tensile strength $R_r$, was determined using the Brazilian test in accordance with [13], yielding values ranging from 0.22 to 0.37 MPa. Tensile strength imposes an important constraint on the behaviour of excavation roofs and zones adjacent to excavation boundaries, where tensile stresses may develop. Under such conditions, local fracture opening and layer detachment may occur.

Uniaxial compression tests, from which $R_c$ and $E_{50}$ were determined, were conducted under two moisture conditions: (i) at the natural moisture content (15 specimens) and (ii) after drying to a constant mass (12 specimens). This approach was adopted to quantify the weakening of chalk under the elevated moisture conditions typical of historic underground workings. At the natural moisture content $R_c$ ranged from 1.47 to 3.18 MPa, whereas drying resulted in a marked increase to 4.88–14.16 MPa. The greater variability in the uniaxial compressive strength of specimens dried to a constant mass was probably associated with the increased influence of heterogeneities induced or accentuated by the drying process. Similarly $E_{50}$ increased from 167.96–747.74 MPa at the natural moisture content to 532.36–1725.11 MPa after drying. These results confirm that moisture content is an important factor governing the load-bearing capacity and deformability of chalk.

**Rock-Mass Parameters**

To determine the quality of the rock mass, characteristic values of the physical and mechanical parameters were adopted in accordance with Eurocode 7 [17], i.e., values for which the probability of a less favourable value occurring does not exceed 5%. The characteristic values were determined statistically using Student's t-distribution for a small sample. For a dataset comprising (N = 15 specimens), the following values were obtained: $R_{c,k}$ = 1.83 MPa, $E_{50,k}$ = 291.83 MPa, and $R_{r,k}$ = 0.26 MPa. For the unit weight (N = 30), a characteristic value of $\gamma_k$ = 19.13 kN/m³ was adopted. These values provided the input parameters for the $RMR_{89}$ and GSI classifications, which were subsequently used to derive rock-mass properties from the laboratory-scale intact-rock parameters.

The overall characteristics of the rock mass were estimated using two geotechnical classification systems: Bieniawski's Rock Mass Rating ($RMR_{89}$) system [18] and the Hoek–Brown Geological Strength Index (GSI) system [19]. These classification systems account for the effects of discontinuities, their surface conditions, and rock-mass structure on its mechanical behaviour. Based on field observations and expert assessment, the respective classification values were determined (Supplementary Fig. S4).

For the analysed section of the underground workings, values of $RMR_{89}$ = 53 (Class III—fair rock) and GSI = 56 (blocky structure with discontinuity surfaces of fair quality) were obtained.

**TLS-Based Geometry Reconstruction and Development of the Three-Dimensional Numerical Model**

High-resolution terrestrial laser scanning was employed to accurately reproduce the geometry of the underground structure in the numerical model. This approach is particularly useful for analysing structures with irregular cross-sections (Supplementary Fig. S5), for which conventional surveying methods do not provide sufficient geometric detail for stability analyses. In recent years, similar approaches combining TLS or SfM data with three-dimensional finite element modelling and safety-assessment procedures have been widely applied to historic underground structures excavated in weak sedimentary rocks [7].

A total of 154 scans were acquired within the Chełm Chalk Tunnels, each comprising approximately 44 million points with X, Y, and Z coordinates. The individual scanning stations were registered using target markers that provided reference points between scans acquired at different locations. Owing to the large volume of observations, the data required sequential processing, including noise filtering, removal of outliers, and point-cloud decimation to a resolution appropriate for the numerical analyses.

In addition, a visualisation model (virtual tour) was developed to support the identification of zones with complex geometry and the selection of areas for numerical analysis (Supplementary Fig. S6). A key challenge, typical of underground structures, was the limited scope for automating the conversion of raw data into analysis-ready geometry. Scanning shadows, narrow passages, and local gaps in surface data required engineering review and manual refinement during the geometry-processing stage.

The excavation geometry was represented by a triangulated irregular network (TIN) generated from the point cloud. The mesh was initially created in MeshLab and subsequently refined in a CAD environment. This process included closing local gaps, removing degenerate elements, and simplifying excessively dense regions. Selected sections of the underground workings—particularly the area beneath the market square and representative chambers—were then extracted from the complete dataset. Geometry verification and segmentation were performed using CloudCompare (Supplementary Fig. S7).

On this basis, a computational model was developed that included both the excavation voids and a sufficiently extensive volume of the surrounding rock mass to minimise the influence of the model boundaries. The volumetric mesh was generated in MIDAS GTS NX, with local refinement applied in areas of complex geometry and anticipated stress concentrations, including roofs, corners, constrictions, and chamber–pillar interfaces. A coarser mesh was used in zones located farther from the excavations. The numerical calculations were performed using FLAC3D to determine the stress and displacement fields and to identify yield zones and other potentially critical areas. The complete modelling workflow is presented in Supplementary Fig. S8.

**Development of the 3D Numerical Model and Computational Scenarios**

The three-dimensional computational model was developed using the excavation geometry obtained from terrestrial laser scanning and the ground-surface topography derived from LiDAR survey data. The model covers an area of 145.0 m × 155.0 m, with its height varying from 17.3 to 28.9 m depending on the local ground-surface elevation and the position of the excavation roofs (Supplementary Fig. S9). The adopted dimensions were sufficient to minimise the influence of the boundary conditions on the analysed area.

The model incorporates the system of underground passages and chambers, the overburden, and anthropogenic loads associated with buildings and land use at the ground surface. The boundary conditions were defined by constraining velocity in the direction normal to each lateral boundary. At the base of the model, velocities in the x, y, and z directions were constrained. The applied boundary conditions are indicated in Supplementary Fig. S9.

The topography was generated from LiDAR survey data obtained from Geoportal [20]. Information on the locations of buildings in the immediate vicinity of the market square was obtained from the same source, enabling the reconstruction of the external foundation outlines through which structural loads are transferred to the rock mass (Supplementary Fig. S10).

Loads from eighteen tenement buildings were applied to foundations extending to approximately 1.5 m below ground level, in accordance with the estimated values presented in Supplementary Fig. S11. In addition, vehicular traffic on the overlying market square was represented by a uniformly distributed surcharge of 25 kPa (Supplementary Fig. S11).

The numerical mesh comprised 2.19 million tetrahedral zones of variable size. Local mesh refinement was applied in the vicinity of the building foundations, underground passages, and chambers. The mesh density was gradually reduced with increasing distance from the area of interest.

Some of the passages, shown in grey in Supplementary Fig. S12, were reinforced with support structures installed after excavation. A review of the archival documentation revealed that some of the original underground passages had partially collapsed and were subsequently reconstructed and reinforced. Accordingly, the support structures were introduced into the model only at the stability-assessment stage, i.e., after the initial stress state had been established and the excavation voids had been created. This modelling sequence enabled the development of a secondary stress and deformation state. The support was represented by shell structural elements with a thickness of 0.40 m and a Young’s modulus of E = 20 GPa. Owing to the lack of complete information regarding the structural behaviour of the various support solutions, a single equivalent support type was adopted. Its purpose was to reproduce the supporting effect and consequently obtain factors of safety greater than 2.0 in the reinforced sections [21].

The numerical analyses were performed using the Hoek–Brown failure criterion. Stability was assessed using the shear-strength reduction method (SRM), in which the shear-strength parameters are progressively reduced until a specified failure criterion is exceeded, based, for example, on velocity,

displacement, or maximum shear strain. The factor of safety (FS) was determined using the velocity criterion and interpreted in relation to the relevant roof–sidewall–pillar failure mechanism. In addition, the strength–stress ratio (SSR) was used as a measure of local stress utilisation. This parameter enabled the identification of areas in which the ratio of available strength to mobilised stress approached a critical value. Owing to the shallow depth of the excavations and the uncertainty associated with the in situ stress field, two values of the mean lateral earth-pressure coefficient, $\bar{\lambda} = 0.8$ and $\bar{\lambda} = 1.2$, were adopted as bounding scenarios for the sensitivity analysis.

The numerical calculations were conducted in the following stages: 1) Initialisation of the primary stress state within the rock mass. 2) Resetting of displacements; introduction of the foundations as an elastic medium; application of the building loads; and removal of the material within the foundation outlines after equilibrium of the initial stress state had been achieved. 3) Application of the vehicular-traffic surcharge to the market square. 4) Resetting of displacements and simulation of the underground excavations. 5) Installation of the support structures in selected passages; replacement of the elastic foundation material with a Mohr–Coulomb material model incorporating artificially high strength parameters; and determination of the factors of safety (FS) and stress-utilisation maps.

This sequence minimises convergence problems, enables the influence of surface loads on the stress state to be evaluated, and allows the effects of excavation geometry to be distinguished from those of subsequently installed reinforcement when interpreting the stability indices.

**General Assessment of the Current Condition of the Analysed Area of the Chełm Chalk Tunnels**

The chambers located adjacent to the “Bieluch” Chamber (Supplementary Fig. S13) were selected for detailed assessment. These chambers are currently closed to visitors and have no structural support.

Field observations indicate local detachment of chalk blocks from the roofs and sidewalls, as well as the accumulation of rock debris on the excavation floors. The chambers have relatively small cross-sectional dimensions, with local heights of up to approximately 3.0 m and widths of approximately 2.5 m. However, they extend vertically for approximately 16 m and are connected by narrow passages, some of which are only approximately 1.0 m high. Their cross-sections are predominantly elliptical, with the major axis oriented vertically.

The groundwater conditions were classified as “damp” according to the RMR89 system, and condensation was observed. This is particularly relevant given the known susceptibility of chalk to moisture-induced weakening. In their current condition, the chambers exhibit no evidence of imminent global instability. Nevertheless, local block detachments pose a hazard to users. Over the long term, progressive weathering and changes in moisture conditions may promote the development of weakened zones and local collapses and, owing to the shallow depth of the workings, may also cause discontinuous deformation at the ground surface.

The current condition of the analysed chambers is shown in Supplementary Fig. S2.

# Abbreviations

CAD
Computer—Aided Design
FEM
Finite Element Method
FLAC3D
Fast Lagrangian Analysis of Continua in Three Dimensions
FS
Factor of Safety
GSI
Geological Strength Index
LiDAR
Light Detection and Ranging
RMR
Rock Mass Rating
SfM
Structure from Motion
SRM
Shear—Strength Reduction Method
SSR
Strength—Stress Ratio
TIN
Triangulated Irregular Network
TLS
Terrestrial Laser Scanning.

# Declarations

Data Availability

The data supporting the findings of this study are provided in the Supplementary Information.

Author contributions

The authors report the following shares of contribution: Mateusz Blajer, 50%; Wioletta Podwyszyńska-Sałosz, 30%; Krzysztof Tajduś, 20%. Mateusz Blajer is the corresponding author.

M.B. and W.P.-S. conducted the field investigations and collected samples for laboratory testing. W.P.-S. performed the laboratory tests, interpreted the results of the field investigations and laboratory tests, and developed the geometric model. M.B. developed the numerical model and performed the numerical simulations. M.B. and K.T. analysed and interpreted the numerical results. K.T. defined the overall scope

and structure of the manuscript and provided scientific supervision throughout the study. M.B. and W.P.-S. prepared the initial draft of the manuscript. K.T. critically reviewed and revised the manuscript. All authors read and approved the final version of the manuscript.

Additional Information

Competing interests

The authors declare no competing interests.

Supplementary information

Supplementary Figures S1–S13 are provided in the accompanying Supplementary Information file.

# References


1. Lafrance, N., Auvray, C., Souley, M. & Labiouse, V. Impact of weathering on macro-mechanical properties of chalk: Local pillar-scale study of two underground quarries in the Paris Basin. *Eng. Geol.* **213**, 107–119. https://doi.org/10.1016/j.enggeo.2016.08.014 (2016).
2. Georgieva, T. et al. Influence of deep coal mines on the stability of shallow cavities. In *Proceedings of the 15th ISRM Congress 2023 and 72nd Geomechanics Colloquium* (eds Schubert, W. & Kluckner, A.) (2023). https://hdl.handle.net/20.500.12907/46320
3. Georgieva, T. et al. Stability assessment of a shallow abandoned chalk mine of Malogne (Belgium). *Eur. J. Environ. Civ. Eng.* **27**, 2358–2372. https://doi.org/10.1080/19648189.2020.1762752 (2023).
4. Trigueros, E., Cánovas, M., Arzúa, J. & Alcaraz, M. Stability of an abandoned siderite mine: A case study in northern Spain. *Open. Geosci.* **13**, 359–376. https://doi.org/10.1515/geo-2020-0240 (2021).
5. Nováková, M. et al. Correcting laser scanning intensity recorded in a cave environment for high-resolution lithological mapping: A case study of the Gouffre Georges, France. *Remote Sens. Environ.* **280**, 113210. https://doi.org/10.1016/j.rse.2022.113210 (2022).
6. Benrabah, A., Senent Domínguez, S., Giraldo, C., Chaves, H. & Rodríguez, C. Jorda Bordehore, L. Stability assessment of the Maltravieso Cave (Caceres, Spain) through engineering rock mass classification, empirical, numerical and remote techniques. *Remote Sens.* **16**, 3883. https://doi.org/10.3390/rs16203883 (2024).
7. Domej, G. et al. High-resolution 3D FEM stability analysis of the Sabereebi Cave Monastery, Georgia. *Rock. Mech. Rock. Eng.* **55**, 5139–5162. https://doi.org/10.1007/s00603-022-02858-z (2022).
8. Meng, Z., Fan, F., Cui, X., Tao, S. & Cao, Y. Numerical modeling and stability analysis of surrounding rock of Yuanjue Cave. *Geofluids* 6652271 (2021). (2021). https://doi.org/10.1155/2021/6652271
9. Agliardi, F., Castellanza, R., Frigerio, G. & Orlandi, G. M. Stability modeling of complex underground mine openings integrating point clouds and FEM 3D. *IOP Conf. Ser. Earth Environ. Sci.* **833**, 012108. https://doi.org/10.1088/1755-1315/833/1/012108 (2021).

10. Hickman, R. J. & Gutierrez, M. S. Formulation of a three-dimensional rate-dependent constitutive model for chalk and porous rocks. *Int. J. Numer. Anal. Methods Geomech.* **31**, 583–605. https://doi.org/10.1002/nag.546 (2007).
11. Hajiabadi, M. R. & Nick, H. M. A modified strain rate dependent constitutive model for chalk and porous rock. *Int. J. Rock. Mech. Min. Sci.* **134**, 104406. https://doi.org/10.1016/j.ijrmms.2020.104406 (2020).
12. Mikoś, T., Chmura, J. & Tajduś, A. *Górniczo-Geotechniczne Metody Adaptacji i Rekonstrukcji Zabytkowych Podziemi*Wydawnictwa AGH, (2014).
13. Ulusay, R. (ed) *The ISRM Suggested Methods for Rock Characterization, Testing and Monitoring: 2007–2014* (Springer International Publishing, 2015).
14. Fabricius, I. L. Chalk: composition, diagenesis and physical properties. *Bull. Geol. Soc. Den*. **55**, 97–128. https://doi.org/10.37570/bgsd-2007-55-08 (2007).
15. Faÿ, O. et al. Chalk marl seams: not quite what they seem … In *Short Papers from the 19th French Congress of Sedimentology, Lille, 2024* ASF Publications 84, 39–42 (French Association of Sedimentologists, 2025). https://doi.org/10.70665/DZYC6363.
16. Jeans, C. V., Wray, D., Lampronti, G. I., Sheikh, H. A. & Evtushenko, A. Origin of flints in the Upper Cretaceous and Danian Chalk of England, Denmark and the North Sea: Evidence from their geological setting, mineralogy, geochemistry, paramagnetic properties and ultrastructure. *Acta Geol. Pol.* **75**, e56. https://doi.org/10.24425/agp.2025.155950 (2025).
17. Polski Komitet Normalizacyjny. Eurocode 7 — Geotechnical Design — Part 1: General Rules PN-EN 1997-1. (2008).
18. Bieniawski, Z. T. *Engineering Rock Mass Classifications: A Complete Manual for Engineers and Geologists in Mining, Civil, and Petroleum Engineering* (Wiley, 1989).
19. Hoek, E., Carter, T. G. & Diederichs, M. S. Quantification of the Geological Strength Index chart. In *47th US Rock Mechanics/Geomechanics Symposium* Vol. 3, 1757–1764 (2013).
20. Geoportal360. Map. https://geoportal360.pl/map. (2020).
21. Hoek, E. *Practical Rock Engineering*Rocscience, (2007).

# Figures

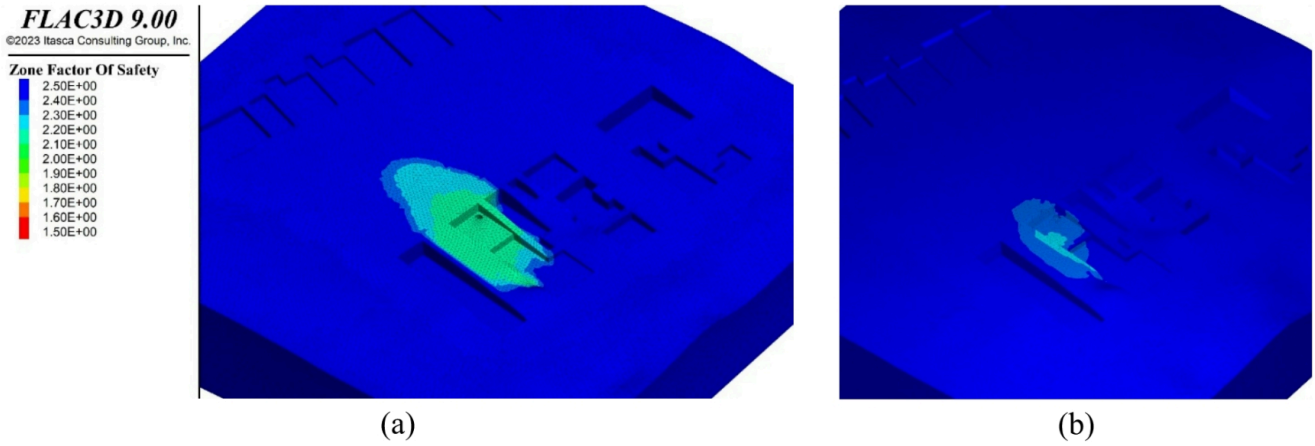



**Figure 1**

Factor-of-safety map for the ground surface: (a) $\bar{\lambda}$ = 0.8; (b) $\bar{\lambda}$ = 1.2—Stage 5

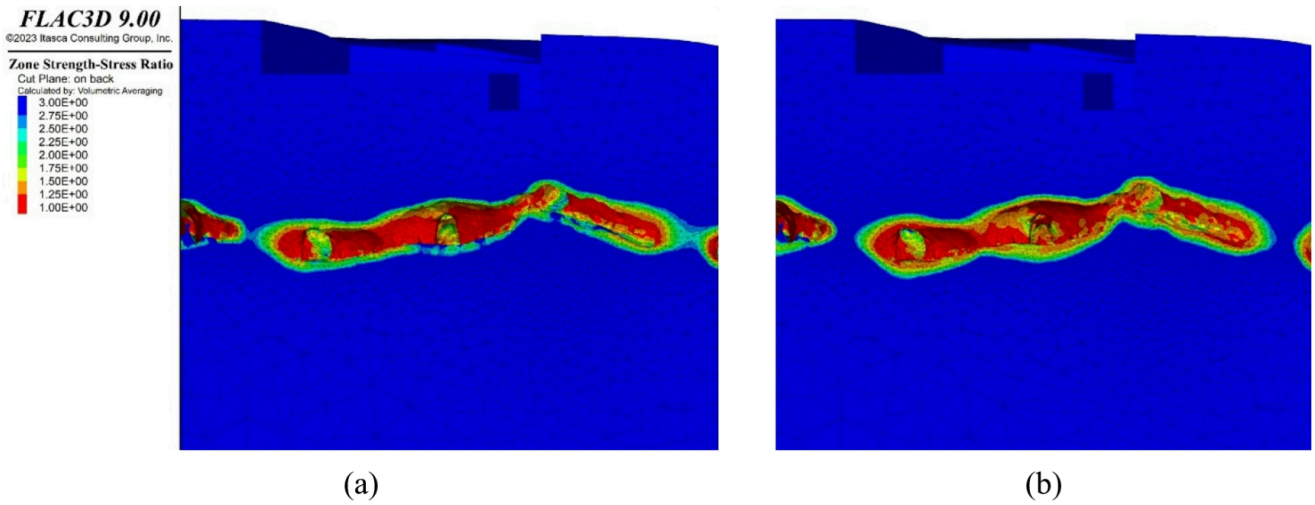



**Figure 2**

Strength–stress ratio in selected cross-sections for: (a) $\bar{\lambda}$ = 0.8; (b) $\bar{\lambda}$ = 1.2—Stage 4, section P1–P1

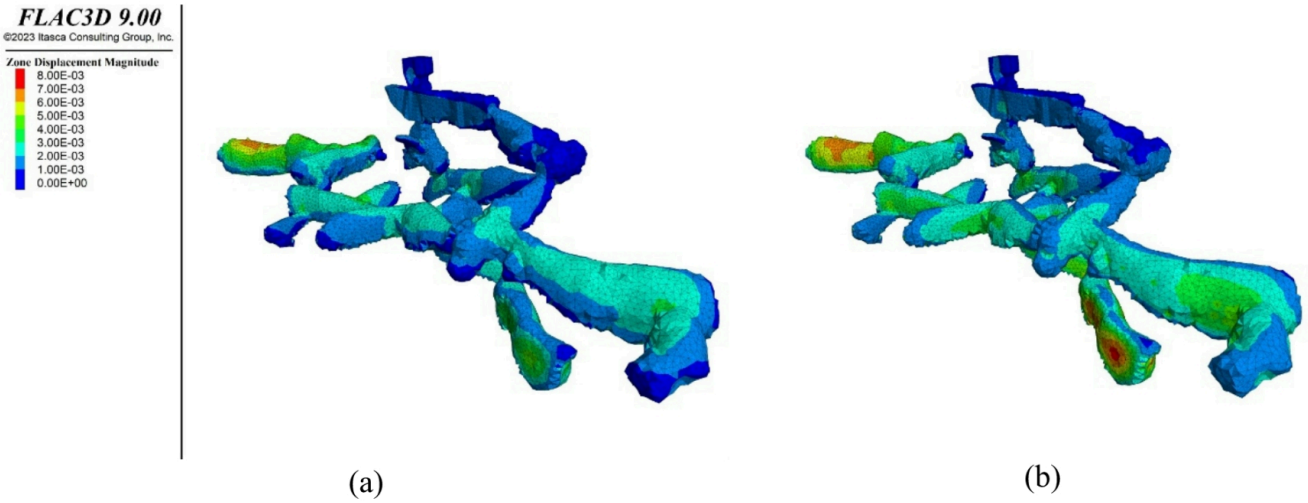



**Figure 3**

Total displacements in the analysed chambers [m]: (a) $\bar{\lambda}$ = 0.8; (b) $\bar{\lambda}$ = 1.2—Stage 4 (view from the “Bieluch” Chamber towards the roof)

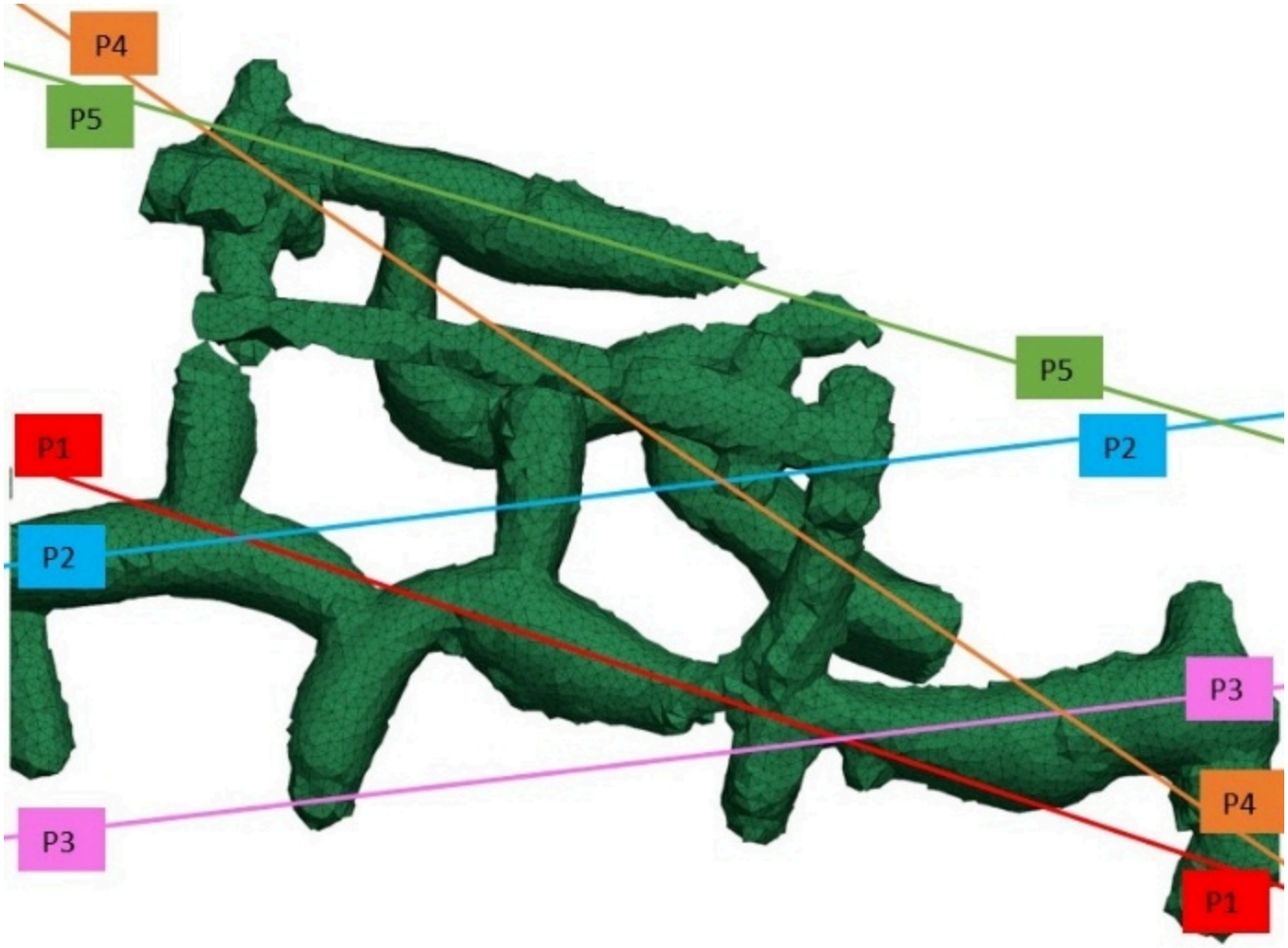
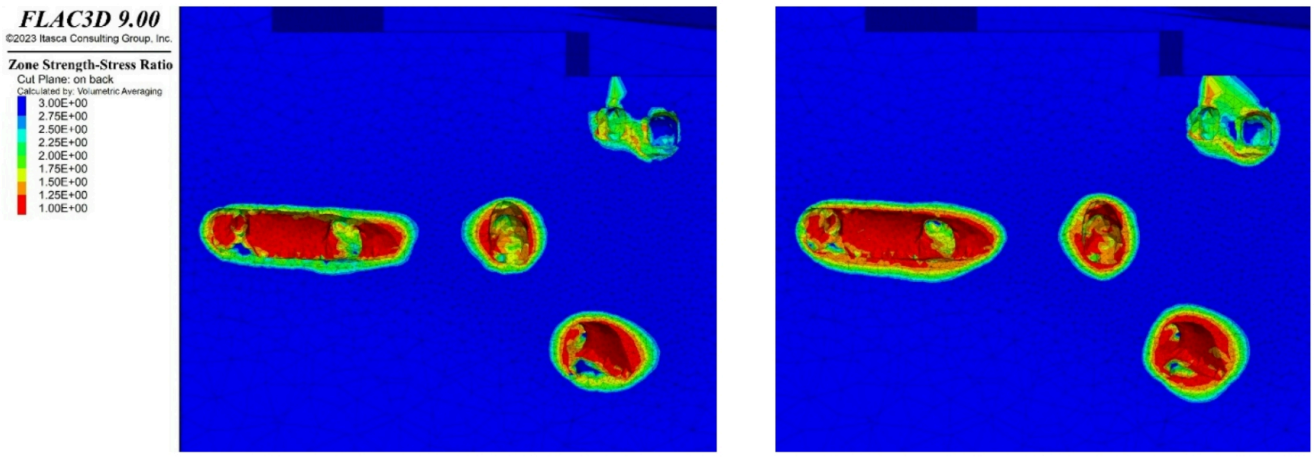



**Figure 4**

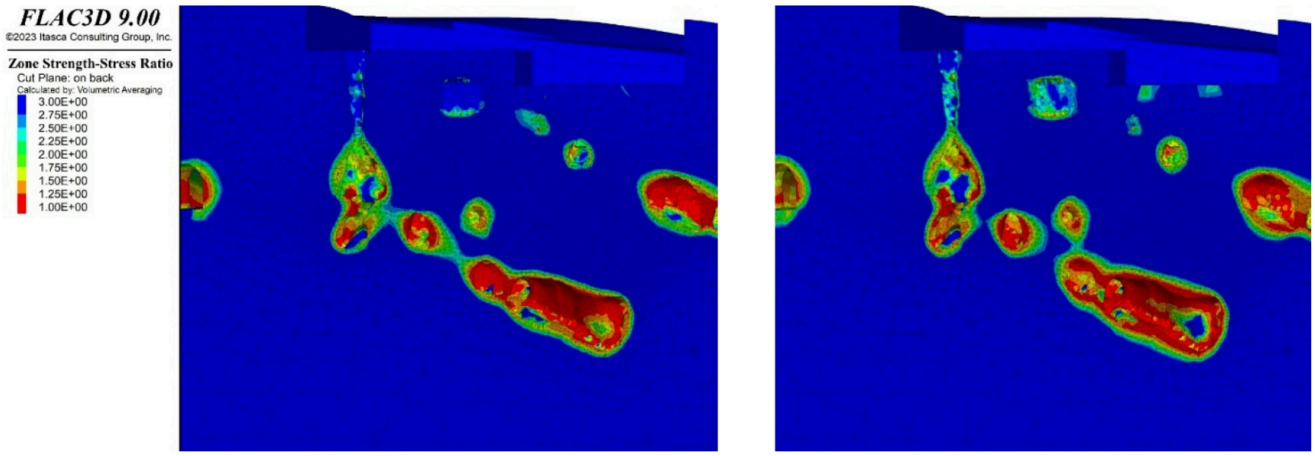
Locations of the cross-sections through the analysed chambers




(a) (b)

**Figure 5**

Strength–stress ratio in selected cross-sections for: (a) $\bar{\lambda}$ = 0.8; (b) $\bar{\lambda}$ = 1.2—Stage 4, section P2–P2




(a) (b)

**Figure 6**

Strength–stress ratio in selected cross-sections for: (a) $\bar{\lambda}$ = 0.8; (b) $\bar{\lambda}$ = 1.2—Stage 4, section P4–P4

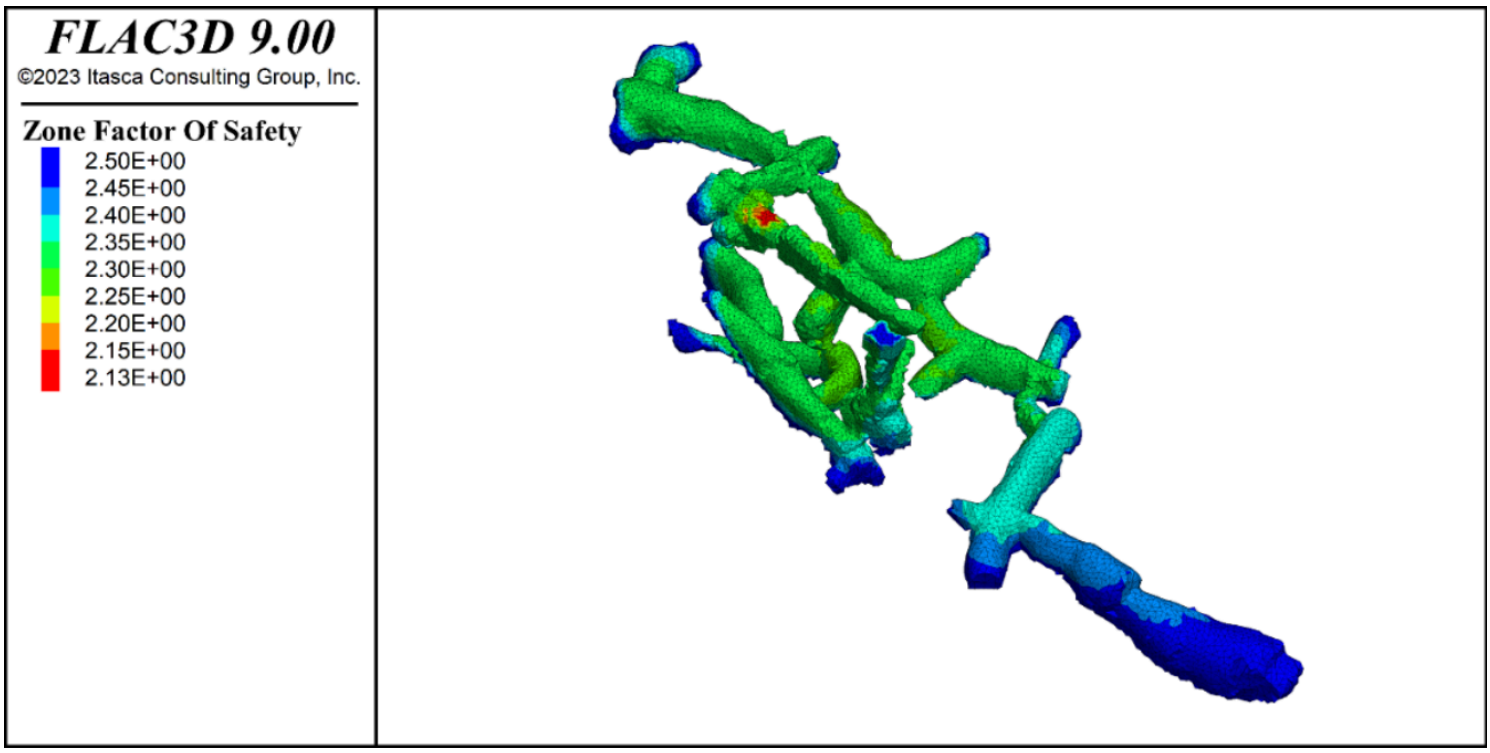



**Figure 7**

Example factor-of-safety map for the analysed chambers ($\bar{\lambda}$ = 0.8—Stage 5)

## Supplementary Files

This is a list of supplementary files associated with this preprint. Click to download.

- SupplementaryInformation.docx